PHYSICAL REVIEW C **96**, 061301(R) (2017)

# Formation and distribution of fragments in the spontaneous fission of $^{240}$Pu

Jhilam Sadhukhan,[1,2,3] Chunli Zhang (张春莉),[3] Witold Nazarewicz,[4] and Nicolas Schunck[5]
[1]*Physics Group, Variable Energy Cyclotron Centre, 1/AF Bidhan Nagar, Kolkata 700064, India*
[2]*Homi Bhabha National Institute, BARC Training School Complex, Anushakti Nagar, Mumbai 400094, India*
[3]*NSCL/FRIB Laboratory, Michigan State University, East Lansing, Michigan 48824, USA*
[4]*Department of Physics and Astronomy, FRIB Laboratory, Michigan State University, East Lansing, Michigan 48824, USA*
[5]*Nuclear and Chemical Science Division, Lawrence Livermore National Laboratory, Livermore, California 94551, USA*
(Received 9 November 2017; published 18 December 2017)

**Background:** Fission is a fundamental decay mode of heavy atomic nuclei. The prevalent theoretical approach is based on mean-field theory and its extensions where fission is modeled as a large amplitude motion of a nucleus in a multidimensional collective space. One of the important observables characterizing fission is the charge and mass distribution of fission fragments.
**Purpose:** The goal of this Rapid Communication is to better understand the structure of fission fragment distributions by investigating the competition between the static structure of the collective manifold and the stochastic dynamics. In particular, we study the characteristics of the tails of yield distributions, which correspond to very asymmetric fission into a very heavy and a very light fragment.
**Methods:** We use the stochastic Langevin framework to simulate the nuclear evolution after the system tunnels through the multidimensional potential barrier. For a representative sample of different initial configurations along the outer turning-point line, we define effective fission paths by computing a large number of Langevin trajectories. We extract the relative contribution of each such path to the fragment distribution. We then use nucleon localization functions along effective fission pathways to analyze the characteristics of prefragments at prescission configurations.
**Results:** We find that non-Newtonian Langevin trajectories, strongly impacted by the random force, produce the tails of the fission fragment distribution of $^{240}$Pu. The prefragments deduced from nucleon localizations are formed early and change little as the nucleus evolves towards scission. On the other hand, the system contains many nucleons that are not localized in the prefragments even near the scission point. Such nucleons are distributed rapidly at scission to form the final fragments. Fission prefragments extracted from direct integration of the density and from the localization functions typically differ by more than 30 nucleons even near scission.
**Conclusions:** Our Rapid Communication shows that only theoretical models of fission that account for some form of stochastic dynamics can give an accurate description of the structure of fragment distributions. In particular, it should be nearly impossible to predict the tails of these distributions within the standard formulation of time-dependent density-functional theory. At the same time, the large number of nonlocalized nucleons during fission suggests that adiabatic approaches where the interplay between intrinsic excitations and collective dynamics is neglected are ill suited to describe fission fragment properties, in particular, their excitation energy.

DOI: 10.1103/PhysRevC.96.061301

*Introduction*. A better understanding of nuclear fission is essential for different branches of basic sciences and applications. Fission governs the existence and stability of heavy and superheavy elements [1–3]. In nuclear astrophysics, fission rates and the related fission fragment distributions are key inputs to investigate the origin of elements heavier than iron [4–6]. Knowledge of fission yields is crucial for the understanding of the production rate of antineutrinos by nuclear reactors [7]. On the applied side, fission data are crucial for, e.g., reactor design, management of the nuclear waste, and international safeguards. Since many nuclei relevant to nuclear astrophysics are very short lived and out of experimental reach, and measurements in specific actinide nuclei for nuclear technology applications can pose safety issues, a predictive theoretical model for nuclear fission is needed.

Theoretical modeling of fission is extremely challenging. Many successful approaches to fission follow the original idea of Bohr and Wheeler [8] that fission is an extreme deformation process typically driven by a few collective variables that characterize the deformation of the nuclear surface, see Refs. [1,2] for examples. Currently, the most commonly used microscopic theoretical approach to fission, rooted in an effective description of nuclear forces among nucleons, is based on nuclear density-functional theory [9]. Here, spontaneous fission (SF) typically is described as a multidimensional quantum tunneling process through the collective space, which takes the nucleus from a ground-state configuration to a very deformed one at the classical outer turning point. This approach, which is, in practice, implemented within the semiclassical Wentzel-Kramers-Brillouin (WKB) approximation, has been successful in describing spontaneous fission half-lives and other properties [10–13].

Calculating the characteristics of the fission fragment themselves, especially their distribution in charge in mass, introduces additional difficulties since it becomes necessary to model explicitly the dynamic from the outer turning point to scission. Although time-dependent density-functional theory methods may seem the most natural to describe this latter phase

 

of the fission process [14,15], each such calculation simulates only a single fission event: Reconstructing entire distributions can become prohibitively expensive especially when pairing correlations are taken fully into account [16]. The situation becomes more complicated for induced fission from excited states where pairing is quenched and dynamics becomes strongly dissipative and nonadiabatic [17]. In this regime, stochastic transport theories have been applied successfully to describe the energy transfer between the collective and the intrinsic degrees of freedom of the fissioning nucleus [2,18–20]. Among such theories, dynamical approaches based on the Langevin equation and its derivatives have been successful in reproducing fission dynamics, including fission yields [20–25].

*Theoretical framework*. In a previous work [26], we outlined a method to calculate spontaneous-fission fragment distributions by combining the multidimensional minimization of the collective action, which produces tunneling rates, with stochastic Langevin dynamics to track fission trajectories from the outer turning point down to scission. The minimization of the action requires computing an adiabatic potential energy and the associated collective inertia in the multidimensional collective space that characterizes fission. We demonstrated that this two-step WKB and Langevin approach provides good agreement with experimental SF yields of $^{240}$Pu and that the predictions are relatively robust with respect to changes in the dissipation tensor, ground-state zero-point energy, and the scission criterion.

We model the collective dynamics of the fissioning system from the outer turning point to scission as a stochastic process involving the interplay between the adiabatic collective motion and the heat bath constituted of intrinsic degrees of freedom of the nucleons. This model is realized effectively by solving the classical Langevin equations with both dissipative and random forces in addition to the standard Newtonian dynamics of collective variables. As a result of stochasticity, a single initial condition on the potential-energy surface (PES) gives rise to a distribution of collective trajectories (because of the random force in the Langevin equation, each such trajectory is unique). We can define the local density of Langevin tracks by counting the number of trajectories in each small surface element $dS$ of the potential-energy surface [27]. We then may define an effective fission path (EFP) by connecting the locus of maxima in densities of Langevin trajectories. The concept of the EFP is illustrated in Fig. 1(a), and 11 EFPs considered in this Rapid Communication are shown in Fig. 1(b). The EFP gives the most probable fragmentation corresponding to the associated initial configuration. The EFPs are calculated for different initial points on the outer turning-point line. As a reminder, the latter is determined from the WKB boundary condition on the two-dimensional potential-energy surface spanned by the axial quadrupole ($Q_{20}$) and octupole moment ($Q_{30}$). The potential energy and the associated nonperturbative cranking inertia tensor are calculated using the Skyrme energy density functional with the SkM$^*$ parametrization in the particle-hole channel and mixed pairing interaction in the pairing channel; see Ref. [26] for details.

To define prefragments formed inside the fissioning system, we compute the neutron and proton localization functions

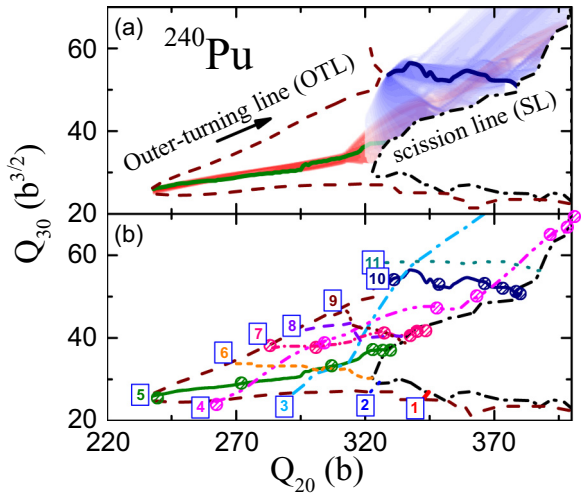


FIG. 1. Top: The density of Langevin trajectories and the corresponding EFPs on the two-dimensional PES on the $(Q_{20}, Q_{30})$ plane. The outer turning-point line (OTL) and the scission line are shown by dashed and dashed-dotted lines, respectively. Bottom: Eleven EFPs considered in this Rapid Communication.

(NLFs) $\mathcal{C}$ for the fissioning nucleus at various prescission configurations along the EFP. As demonstrated in Refs. [28,29], NLFs quantify the degree of clustering more efficiently than nucleonic density distributions. This is because the pattern of concentric rings exhibited by NLFs reflects the underlying shell structure, which is averaged out in density distributions.

Figure 2 shows the typical application of NLFs to prefragment identification for a typical case of an elongated configuration of $^{240}$Pu. The $z$-coordinates $z_L$ and $z_H$, corresponding to the maximum of the radial coordinate $r_\perp(z)$

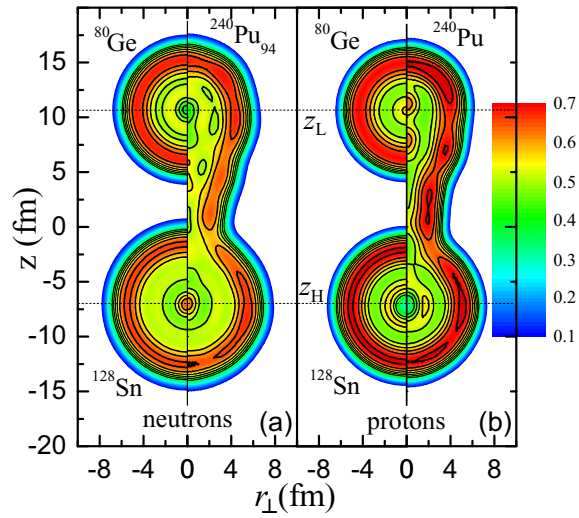


FIG. 2. Neutron (left) and proton (right) localization functions in $^{240}$Pu at ($Q_{20} = 305$ b, $Q_{30} = 32$ b$^{3/2}$) compared to the individual NLFs of the localized prefragments ($^{80}$Ge and $^{128}$Sn). The symmetry axis is marked by the vertical line. The horizontal dotted lines $z_L$ and $z_H$ indicate the position of the maxima of the radial coordinate $r_\perp(z)$ associated with the NLF profile.

associated with the NLF profile, are indicated. We note that the NLFs for $z \geqslant z_{\rm L}$ and $z \leqslant z_{\rm H}$ exhibit characteristic ringlike patterns indicating the presence of localized nucleons inside the elongated $^{240}$Pu. We thus propose to define the localized prefragments by integrating the densities outside the horizontal lines in Fig. 2 (and multiplying the result by 2 to account for reflection symmetry as the general majority of atomic nuclei are reflection symmetric in their ground states). Applied to the case of Fig. 2, such a procedure predicts that the two localized prefragments are $^{128}$Sn and $^{80}$Ge. To estimate how well this method works, we perform independent calculations of ground-state NLFs for these two prefragments. As seen of Fig. 2, there is remarkable agreement between the ground-state NLFs of the prefragments and the NLFs of $^{240}$Pu as far as the ring pattern is concerned. It is worth noting that a fairly similar technique, based on density comparison, has been applied successfully in Refs. [30,31] to identify prefragments.

*Results*. For the 11 initial configurations on the outer turning line shown in Fig. 1(b), we have generated an ensemble of $\approx 10^6$ Langevin tracks. We then have extracted the partial contribution of each EFP to the cumulative mass distribution by weighing the Langevin distributions with the appropriate tunneling probabilities determined by the collective action from the inner turning point to the outer turning point. The partial yield distributions for the heavy fragment mass are plotted in Fig. 3(a) for different initial configurations. As expected, the peaks of the fragment mass distribution shown in Fig. 5 of Ref. [26] are built mostly from EFPs that are near the most probable fission path. On the other hand, the contribution of EFPs that connect the region of large-$Q_{30}$ values at the outer turning line to very asymmetric scission configurations are quenched by small tunneling probabilities. For example, the contribution from EFP11 is practically negligible. Figure 3(a) shows that the tail of the yield distribution comes from EFPs that connect highly probable outer turning points with very asymmetric scission configurations, such as those related to EFP3 and EFP4, for which the potential energy does not decrease monotonically, see Fig. 3(b). For these trajectories, the random force is primarily responsible for the upward motion rather than the collective term.

We now focus on the structural properties of the prefragments. To this end, we select five different configurations along each EFP4, EFP5, EFP7, and EFP10. These configurations, representative of various types of fission structures, are marked in Fig. 1(b) by circles. Figure 4 shows the corresponding neutron NLFs; proton NLFs exhibit very similar features. It is interesting to see that the outer structures (at $z \geqslant z_{\rm L}$ and $z \leqslant z_{\rm H}$) of the fissioning nucleus—associated with prefragments—barely are affected by the increasing shape deformation of the fissioning system; it is the neck that steadily evolves.

We apply the procedure based on NLFs to extract the proton and neutron numbers of the prefragments along the EFPs of Fig. 1(b). The results are shown in Fig. 5. We notice that the particle numbers of the localized prefragments are remarkably stable as the deformation increases. In addition, the spread of this number, indicated by the width of the associated band, becomes fairly narrow at large elongations (less than $\pm 2$ particles). This suggests that the prefragments formed in the initial phase of fission hardly change, and the number of nucleons,

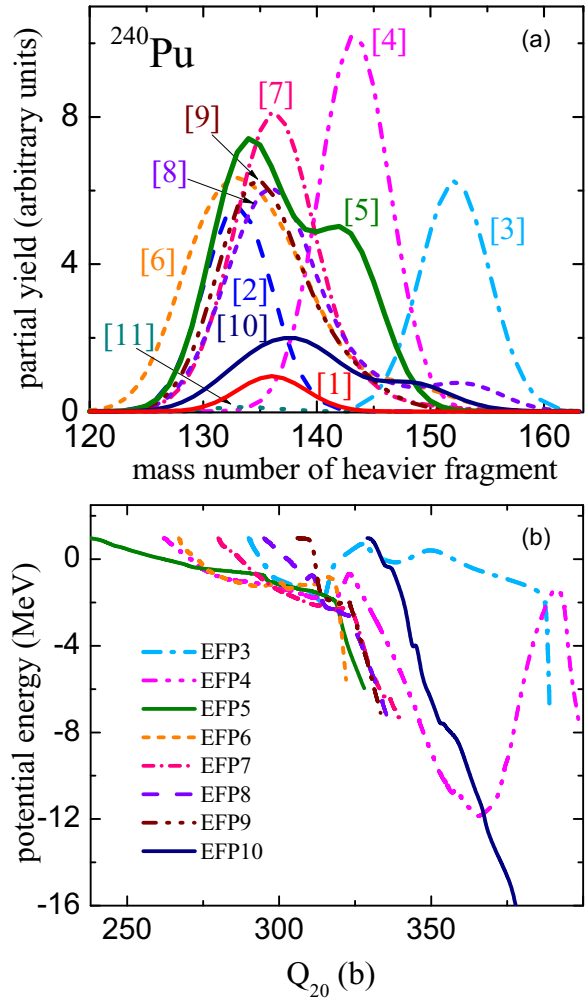


FIG. 3. Top: Partial mass distributions for different initial configurations shown in Fig. 1(b). The contribution from the minimum-action fission path EFP 5 is shown by a thick line. Bottom: The potential energy along each EFP. Note the nonmonotonic behavior for EFP 3 and EFP 4.

which do not belong to prefragments (primarily forming the neck) stays roughly contant in prescission configurations. In the case considered, around 22 neutrons and 12 protons are not localized in the prefragments: They represent the glue that holds the prefragments together. For comparison, we also computed prefragments using the method of Ref. [31] based on the analysis of linear (e.g., radially integrated) nucleonic densities. The NLF-based approach is close to that of Ref. [31]; in most cases, the difference does not exceed two nucleons.

We also have computed the prefragments by integrating the nucleonic densities from the minimum of the neck at $z = z_N$ [32,33]. It is seen that the spread in the associated neutron and proton numbers is appreciably greater than for the prefragments determined by means of NLFs especially at smaller elongations. In this approach, the neck nucleons are associated with individual prefragments; hence, the density-based particle numbers are larger by about 5 (7) protons and 8 (11) neutrons, for the light (heavy) prefragments, respectively. It is to be noted that these numbers are not constant: One can

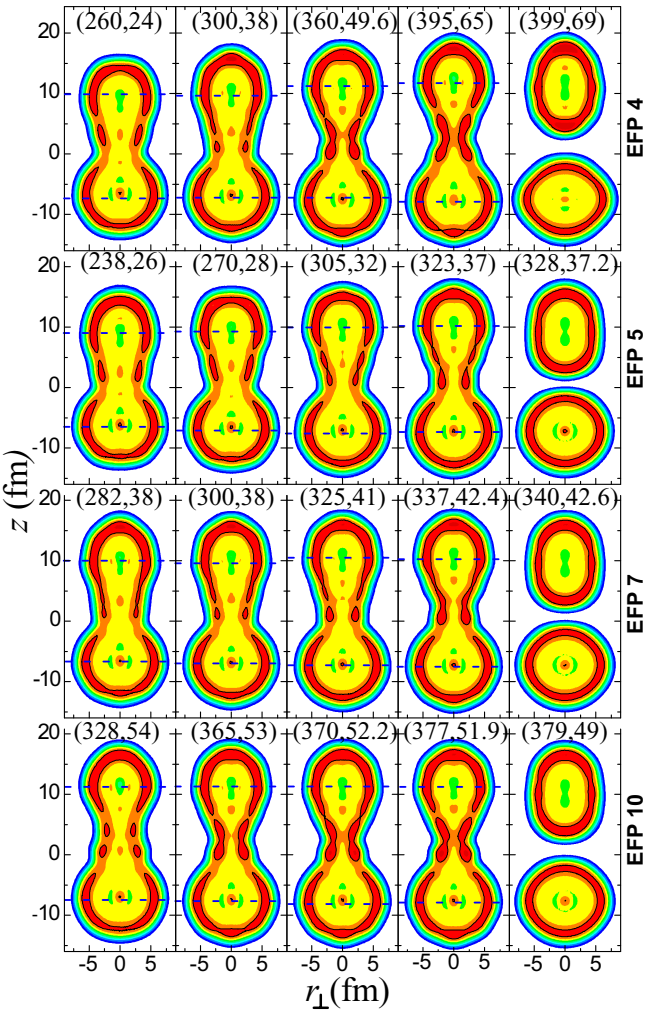


FIG. 4. Neutron NLFs for neutrons for several configurations [indicated by $Q_{20}$ (in barns) and $Q_{30}$ (in $b^{3/2}$)] along the four EFPs indicated. The color legend is same as in Fig. 2. The horizontal dashed lines indicate the position of the maxima of the radial coordinate associated with the NLF profile.

see a gradual transfer of nucleons from the light prefragment to the heavy one as the scission point is approached.

Our result clearly indicates that during the motion of the system between the OTL and scission, the distance between the early-formed prefragments gradually increases, which results in a longer and thinner neck, see Fig. 4. This neck evolution can be illustrated by computing the expectation value of the neck operator $Q_N = \exp[-(z - z_N)^2/a_N^2]$ [33,34]. Figure 6 shows $q_N = \langle Q_N \rangle$ as a function of the EFP length. For all EFPs, $q_N$ gradually decreases prior to scission at which it rapidly vanishes (see also Ref. [31] for a similar analysis).

The above findings reinforce lingering questions about the process of fragmentation in an adiabatic theory of fission. The concept of scission and the criteria used to define it have long been debated in the literature [35–38]. As our NLF-based analysis shows, prefragments are entangled strongly near the scission point, and a full quantum-mechanical treatment most certainly is needed to approach the asymptotic conditions of two well-separated fragments [33,39]. Recent work based

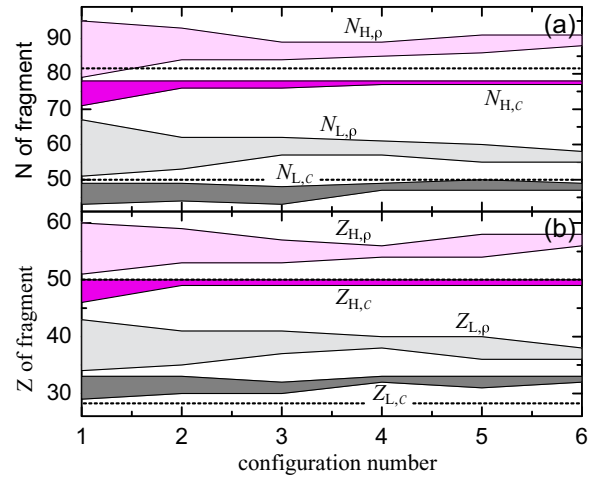


FIG. 5. Upper panel: The ranges for the number of localized (a) neutrons and (b) protons for heavier $(N_{H,C}, Z_{H,C})$ and lighter $(N_{L,C}, Z_{L,C})$ fragments as a function of the configurations along the EFPs marked in Fig. 1(b) by circles. The ranges obtained by integrating the nucleon density for the heavier $(N_{H,\rho}, Z_{H,\rho})$ and lighter $(N_{L,\rho}, Z_{L,\rho})$ fragments from the minimum of the neck. The magic numbers are marked by the horizontal dotted lines.

on time-dependent density-functional theory concludes that nonadiabatic collective dynamics near scission is essential [14–16,40]. To estimate the degree of nonadiabaticity, in Fig. 7 we show the average collective momentum of Langevin trajectories for each EFP together with the collective momentum prior to scission obtained by considering configurations within three time steps from the scission point. It is seen that the average collective momentum just before scission is considerably larger than the average momentum of the collective coordinates outside the OTL.

The mechanism of generating fission yields based on the Langevin framework proposed in Ref. [26] provides results that are consistent with experiment. In this respect, this approach seems to be superior to the method of random neck rupture [31,36], which underestimates the width of mass yields.

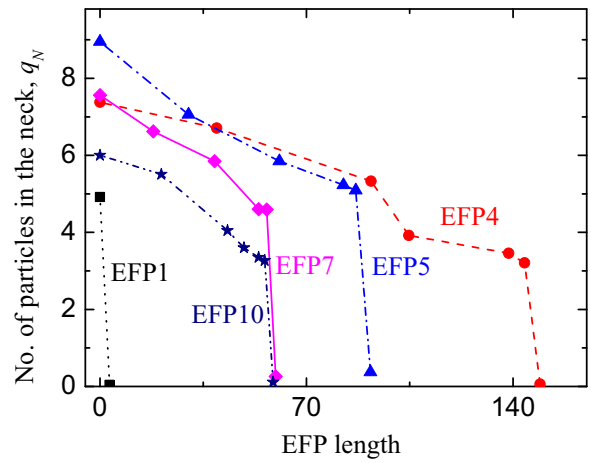


FIG. 6. Number of particles in the neck $q_N = \langle Q_N \rangle$ defined through the expectation value of the neck operator with $a_N = 1$ fm as a function of the length of the EFP.

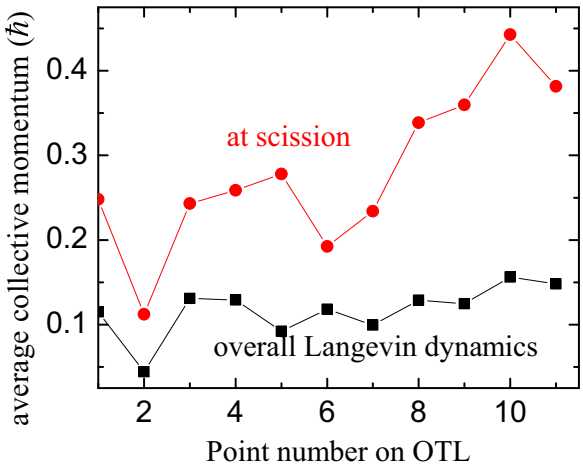


FIG. 7. Average collective momentum of Langevin trajectories for different EFPs (squares) and shortly before reaching the scission point (dots).

*Conclusions*. In this Rapid Communication, we have performed a detailed analysis of the formation and distribution of spontaneous fission yields. We have established that the tails of the fission fragment distributions come from the contributions from Langevin trajectories that connect highly probable outer turning points with very asymmetric scission configurations. The potential energy along such trajectories is often nonmonotonic, and the corresponding Langevin dynamics is impacted greatly by fluctuations. This finding is consistent with the Langevin model analysis [22] that concluded that the width of the fission yields is primarily determined by near-scission fluctuations caused by the random force.

We have also shown that, although the prefragments are formed early and change little as the nucleus deforms, there is a large number of nucleons ($\approx$34) that are not localized in the prefragments even near the scission point. These nucleons have a large impact on the final properties of the fission yields as they are distributed rapidly at scission to the final fragments. The number of these nucleons depends on the neck structure of the concerned nucleus.

Finally, our results suggest that even nonadiabatic time-dependent theories will be challenged to reproduce the tails of the distribution unless a mechanism equivalent to the random force of the Langevin equation is included. Conversely, such theories probably are adapted much more to describing the fast rearrangements of nucleons at scission. Although the stochastic mean-field technique has been developed within time-dependent density-functional theory [41,42], it is only very recently that it has been applied to fission fragment properties [43].

*Acknowledgments.* This work was supported by the U.S. Department of Energy under Awards No. DOE-DE-NA0002574 (NNSA, the Stewardship Science Academic Alliances Program) and No. DE-SC0008511 (Office of Science, Office of Nuclear Physics NUCLEI SciDAC-3 Collaboration). Part of this research also was performed under the auspices of the U.S. Department of Energy by Lawrence Livermore National Laboratory under Contract No. DE-AC52-07NA27344. Computational resources were provided through an INCITE award "Computational Nuclear Structure" by the National Center for Computational Sciences (NCCS), and by the National Institute for Computational Sciences (NICS). Computing support for this Rapid Communication also came from the Lawrence Livermore National Laboratory (LLNL) Institutional Computing Grand Challenge Program.

[1] S. Bjørnholm and J. E. Lynn, Rev. Mod. Phys. **52**, 725 (1980).
[2] H. J. Krappe and K. Pomorski, *Theory of Nuclear Fission: A Textbook* (Springer, New York, 2012).
[3] Y. T. Oganessian and V. K. Utyonkov, Rep. Prog. Phys. **78**, 036301 (2015).
[4] G. Martínez-Pinedo, D. Mocelj, N. Zinner, A. Kelić, K. Langanke, I. Panov, B. Pfeiffer, T. Rauscher, K.-H. Schmidt, and F.-K. Thielemann, Prog. Part. Nucl. Phys. **59**, 199 (2007).
[5] S. Goriely, J.-L. Sida, J.-F. Lemaître, S. Panebianco, N. Dubray, S. Hilaire, A. Bauswein, and H.-T. Janka, Phys. Rev. Lett. **111**, 242502 (2013).
[6] S. A. Giuliani, G. Martínez-Pinedo, and L. M. Robledo, arXiv:1704.00554.
[7] F. P. An *et al.* (Daya Bay Collaboration), Phys. Rev. Lett. **118**, 251801 (2017).
[8] N. Bohr and J. A. Wheeler, Phys. Rev. **56**, 426 (1939).
[9] N. Schunck and L. M. Robledo, Rep. Prog. Phys. **79**, 116301 (2016).
[10] A. Staszczak, A. Baran, and W. Nazarewicz, Phys. Rev. C **87**, 024320 (2013).
[11] S. A. Giuliani, L. M. Robledo, and R. Rodríguez-Guzmán, Phys. Rev. C **90**, 054311 (2014).
[12] S. A. Giuliani and L. M. Robledo, Phys. Rev. C **88**, 054325 (2013).
[13] H. Tao, J. Zhao, Z. P. Li, T. Nikšić, and D. Vretenar, Phys. Rev. C **96**, 024319 (2017).
[14] C. Simenel and A. S. Umar, Phys. Rev. C **89**, 031601(R) (2014).
[15] G. Scamps, C. Simenel, and D. Lacroix, Phys. Rev. C **92**, 011602 (2015).
[16] A. Bulgac, P. Magierski, K. J. Roche, and I. Stetcu, Phys. Rev. Lett. **116**, 122504 (2016).
[17] W. Nörenberg, Nucl. Phys. A **409**, 191 (1983).
[18] Y. Abe, S. Ayik, P.-G. Reinhard, and E. Suraud, Phys. Rep. **275**, 49 (1996).
[19] Y. Abe, C. Grégoire, and H. Delagrange, J. Phys., Colloq. **47**, C4-329 (1986).
[20] A. J. Sierk, Phys. Rev. C **96**, 034603 (2017).
[21] P. Fröbrich and I. Gontchar, Phys. Rep. **292**, 131 (1998).
[22] Y. Aritomo, S. Chiba, and F. Ivanyuk, Phys. Rev. C **90**, 054609 (2014).
[23] P. Möller and J. Randrup, Phys. Rev. C **91**, 044316 (2015).
[24] V. Denisov, T. Margitych, and I. Sedykh, Nucl. Phys. A **958**, 101 (2017).
[25] K. Mazurek, P. N. Nadtochy, E. G. Ryabov, and G. D. Adeev, Eur. Phys. J. A **53**, 79 (2017).
[26] J. Sadhukhan, W. Nazarewicz, and N. Schunck, Phys. Rev. C **93**, 011304 (2016).

[27] S. Pal, G. Chaudhuri, and J. Sadhukhan, Nucl. Phys. A **808**, 1 (2008).
[28] P.-G. Reinhard, J. A. Maruhn, A. S. Umar, and V. E. Oberacker, Phys. Rev. C **83**, 034312 (2011).
[29] C. L. Zhang, B. Schuetrumpf, and W. Nazarewicz, Phys. Rev. C **94**, 064323 (2016).
[30] M. Warda, A. Staszczak, and W. Nazarewicz, Phys. Rev. C **86**, 024601 (2012).
[31] M. Warda and A. Zdeb, Phys. Scr. **90**, 114003 (2015).
[32] W. Younes and D. Gogny, Phys. Rev. C **80**, 054313 (2009).
[33] N. Schunck, D. Duke, H. Carr, and A. Knoll, Phys. Rev. C **90**, 054305 (2014).
[34] J. F. Berger, J. D. Anderson, P. Bonche, and M. S. Weiss, Phys. Rev. C **41**, R2483(R) (1990).
[35] K. T. R. Davies, R. A. Managan, J. R. Nix, and A. J. Sierk, Phys. Rev. C **16**, 1890 (1977).
[36] U. Brosa, S. Grossmann, and A. Müller, Phys. Rep. **197**, 167 (1990).
[37] L. Bonneau, P. Quentin, and I. N. Mikhailov, Phys. Rev. C **75**, 064313 (2007).
[38] M. Rizea and N. Carjan, Nucl. Phys. A **909**, 50 (2013).
[39] W. Younes and D. Gogny, Phys. Rev. Lett. **107**, 132501 (2011).
[40] Y. Tanimura, D. Lacroix, and G. Scamps, Phys. Rev. C **92**, 034601 (2015).
[41] S. Ayik, Phys. Lett. B **658**, 174 (2008).
[42] D. Lacroix and S. Ayik, Eur. Phys. J. A **50**, 95 (2014).
[43] Y. Tanimura, D. Lacroix, and S. Ayik, Phys. Rev. Lett. **118**, 152501 (2017).